*J. Fluid Mech.* (1987), *vol.* 180, *pp.* 475–494
*Printed in Great Britain*



# The rheology of dilute suspensions of slender rods in weak flows

By DOUGLAS H. BERRY† AND WILLIAM B. RUSSEL
Department of Chemical Engineering, Princeton University, Princeton, NJ 08544, USA

(Received 26 March 1986 and in revised form 25 November 1986)

This paper describes the consequences of pair interactions in dilute suspensions of rigid rods of length $2l$ and radius $a$ subjected to weak, steady shear flows. The combination of hydrodynamic and Brownian forces increases alignment with the flow, thereby enhancing the shear thinning and strain thickening expected from dilute theories. The theory is asymptotic in $Pe \ll 1$ and $\epsilon = (\ln 2l/a)^{-1} \ll 1$ but requires an *ad hoc* approximation to simplify the form of the hydrodynamic interactions and the rod–rod excluded volume. The theoretical predictions of the Huggins coefficient in simple shear flow are compared with data in the literature for Xanthan gum, a semi-rigid biopolymer. Comparison with semi-dilute theories emphasizes the fundamentally different nature of the interactions in the two regimes and indicates that the transition between the two lies in the range $1.5 \leqslant [\eta]_0 n \leqslant 6$.

## 1. Introduction

Existing analyses of the rheology of suspensions of slender rods, whether representing colloidal particles or rigid macromolecules, concentrate on either infinite dilution (e.g. Hinch & Leal 1972; Brenner 1974) or semi-dilute concentrations (Doi & Edwards 1978*a*, *b*; Jain & Cohen 1981). The former completely neglect interactions and, therefore, require $nl^3 \ll 1$ ($n$ = number density, $2l$ = length). The latter assume $1 \ll nl^3 \ll (l/a)^2$ ($a$ = radius of rod) and account for interactions via a physically compelling but, nonetheless, *ad hoc* representation of the hindered diffusion process. Here we examine in detail pair interactions between rods suspended in a Newtonian fluid to determine the $O(nl^3)^2$ contribution to the bulk stress in the dilute limit and to provide some perspective for assessing interactions in the transition between the dilute and semi-dilute regimes.

The motivation for studying moderately concentrated suspensions of rods comes from the behaviour of water-soluble polymers used as thickeners in coatings and for mobility control in enhanced oil-recovery operations, and the importance of rigid polymers in the fabrication of high-modulus fibres (Chu *et al.* 1981). Low-molecular-weight carboxymethyl cellulose, for example, becomes a fully extended rod at ionic strengths below $10^{-1}$ M (Moan & Wolff 1974). Xanthan gum, on the other hand, is not completely rigid (Holzwarth 1978) but sufficiently stiff to behave in dilute solution much like a rigid rod even at high ionic strengths (Whitcomb & Macosko 1978). The rigidity as well as the presence of fixed charges along the backbone of such macromolecules amplify both the importance of interactions at moderate concentrations ($nl^3 = O(1)$) and their dependence on the solution chemistry. Hence, as with colloidal suspensions (Russel 1980), pair interactions should provide a physical basis

† Present address: Georgia-Pacific Resins, Inc., 1754 Thorne Road, Tacoma, WA 98421, USA.

for understanding more concentrated solutions where interactions dominate both the thermodynamics and the rheology.

Construction of a pair-interaction theory for rods requires expressions for (i) the hydrodynamic and thermodynamic interactions, (ii) the microstructure as characterized by the orientation distribution function and (iii) the resulting bulk stress. Our analysis (§2) employs slender-body theory (Batchelor 1970*b*) to describe the hydrodynamics of rods. The interactions are weak but long ranged, so we construct a regular perturbation expansion in $\epsilon = [\ln(2l/a)]^{-1} \ll 1$, retaining only the $O(\epsilon)$ term. To obtain tractable expressions these are simplified to the far-field form. Then the velocities and induced dipole for one rod can be written in terms of the undisturbed velocity field plus the disturbance generated by a second rod. The equation governing the orientation distribution function is derived in §3 from the $N$-particle conservation equation by integrating over the configurations of $N-1$ particles in the manner of Hinch (1977) and Rallison & Hinch (1986). The long-range hydrodynamic interaction produces a non-convergent integral which we renormalize as suggested by Batchelor (Batchelor & Green 1972; Batchelor 1977). The effect of the second rod on the first then resembles an enhanced rate of strain, expressed as an integral over the surface of the rod–rod excluded volume. A solution valid for weak flows is obtained as a regular perturbation expansion in the Péclet number, $Pe \ll 1$, carried out to $O(Pe^3)$ to capture the normal stresses, shear thinning, and strain thickening arising from alignment of the rod in the direction of flow.

Explicit evaluation of the orientation distribution function requires, however, dealing with the complex geometry of the excluded volume. Here (§4) we resort to pre-averaging this volume over the orientations of both rods, a second *ad hoc* approximation similar to taking the far-field limit for the hydrodynamic interactions. The result is a slightly deformed sphere with a shape dependent on the Péclet number. Thus the theory is asymptotic in $\phi \ll 1$, $\epsilon \ll 1$ and $Pe \ll 1$ but contains an $O(1)$ error due to the far-field and pre-averaging approximations.

Sections 5 and 6 contain the derivation and evaluation of the bulk stress, including both Brownian and hydrodynamic contributions. The long-range hydrodynamic interaction again produces a non-convergent integral which is renormalized by the standard technique (Batchelor & Green 1972). Explicit results for the bulk stress to second order in the Péclet number are given for both simple shear and extensional flows.

The final two sections compare the theoretical results with experimental data on the viscosity of dilute solutions of Xanthan gum (Chauvateau 1982) and with predictions from hindered-diffusion theories for semi-dilute concentrations (Doi & Edwards 1978*a*, *b*). The dilute theory matches the experimental data at zero shear, but is only qualitatively similar at higher shear. Comparison with the hindered-diffusion theory at zero shear reveals a transition between the two for $6 \leqslant \frac{4}{3}\pi n l^3 \epsilon \leqslant 24$.

## 2. Dynamics of interacting rods

The motion of a slender rigid rod of radius $a$ and length $2l \gg a$ suspended in a fluid of viscosity $\mu$ is described quite conveniently by slender-body theory (Batchelor 1970*b*). Here we consider only terms of leading order in

$$\epsilon = \left(\ln\frac{2l}{a}\right)^{-1} \ll 1,$$

which are independent of the exact geometry, i.e. the variation of radius with axial position. All quantities will be dimensionless, scaled on the following:

$$\begin{aligned} &\text{length} && l, \\ &\text{velocity} && l(\boldsymbol{E}:\boldsymbol{E})^{\frac{1}{2}}, \\ &\text{force} && \frac{8\pi}{3}\mu l^2(\boldsymbol{E}:\boldsymbol{E})^{\frac{1}{2}}\epsilon, \end{aligned}$$

where $\boldsymbol{E}$ is the macroscopic rate-of-strain tensor. The Péclet number

$$Pe = \frac{8\pi\mu l^3\epsilon(\boldsymbol{E}:\boldsymbol{E})^{\frac{1}{2}}}{3kT}$$

will gauge the importance of shear relative to rotary Brownian motion.

The linearity of the Stokes equations permits the velocity $\boldsymbol{u}$ at position $\boldsymbol{x}$ in the fluid to be represented by a superposition of fundamental solutions,

$$\begin{aligned} \boldsymbol{u}(\boldsymbol{x}) &= \boldsymbol{u}_0(\boldsymbol{x}) + \tfrac{1}{3}\epsilon \int_{-1}^{1} \boldsymbol{f}(s)\cdot\boldsymbol{I}(\boldsymbol{x}-\boldsymbol{x}')\,\mathrm{d}s \\ &\equiv \boldsymbol{u}_0(\boldsymbol{x}) + \boldsymbol{u}'(\boldsymbol{x}). \end{aligned} \tag{1}$$

Here $\boldsymbol{u}_0(\boldsymbol{x})$ is the velocity in the absence of the rod and $\boldsymbol{u}'(\boldsymbol{x})$ is the disturbance due to a rod with orientation $\boldsymbol{q}$ centred at $\boldsymbol{x}_0(\boldsymbol{x}' = \boldsymbol{x}_0 + s\boldsymbol{q})$ expressed in terms of the Oseen tensor

$$\boldsymbol{I}(\boldsymbol{r}) = \frac{\boldsymbol{\delta}}{r} + \frac{\boldsymbol{rr}}{r^3}, \tag{2}$$

where $\boldsymbol{\delta}$ is the isotropic tensor. The force per unit length $\boldsymbol{f}(s)$ is unknown. The force and torque acting on the rod and the dipole induced in the rod by the flow are respectively related to $\boldsymbol{f}(s)$ by

$$\left.\begin{aligned} \boldsymbol{F} &= \int_{-1}^{1} \boldsymbol{f}(s)\,\mathrm{d}s, \\ \boldsymbol{T} &= \int_{-1}^{1} s\boldsymbol{q}\times\boldsymbol{f}(s)\,\mathrm{d}s, \\ \boldsymbol{S} &= -\boldsymbol{q}\int_{-1}^{1} s\boldsymbol{f}(s)\,\mathrm{d}s. \end{aligned}\right\} \tag{3}$$

The no-slip boundary condition at the surface of the rod requires that

$$\boldsymbol{u} = \boldsymbol{U} + s\dot{\boldsymbol{q}}, \tag{4}$$

where $\boldsymbol{U}$ and $\dot{\boldsymbol{q}}$ are the translational and rotational velocities of the rod, respectively.

The integral equation resulting from (1) and (4) determines $\boldsymbol{f}(s)$, but the quantities of interest, $\dot{\boldsymbol{q}}$ and $\boldsymbol{S}$, can be found to first order in $\epsilon$ without an explicit solution. Instead, multiplication by $\boldsymbol{q}\times(s\boldsymbol{q}\times)$ and integration of the entire integral equation over the length of the rod produces

$$\dot{\boldsymbol{q}} = \frac{3}{2}\int_{-1}^{1} s(\boldsymbol{u}_0 - (\boldsymbol{u}_0\cdot\boldsymbol{q})\,\boldsymbol{q})\,\mathrm{d}s + \boldsymbol{T}\times\boldsymbol{q}. \tag{5}$$

Through similar manipulations

$$\boldsymbol{S} = \tfrac{3}{4}\boldsymbol{qq}\int_{-1}^{1} s(\boldsymbol{u}_0\cdot\boldsymbol{q})\,\mathrm{d}s + \boldsymbol{q}(\boldsymbol{q}\times\boldsymbol{T}). \tag{6}$$

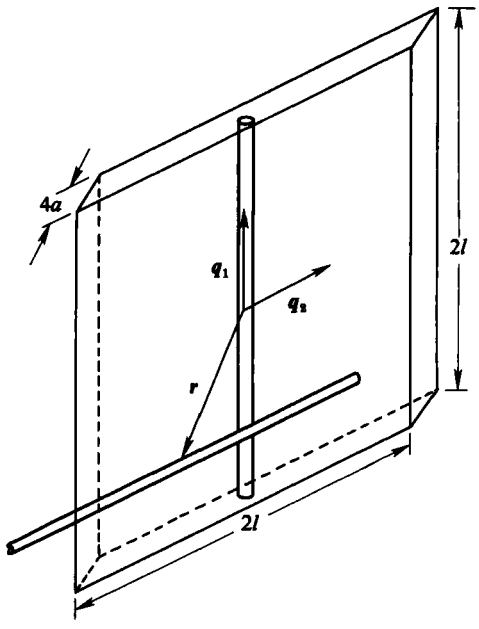


FIGURE 1. Geometry of pair interaction with hard-rod excluded volume.

For two interacting rods (1) represents the fluid velocity exactly if forces are distributed along both axes and the boundary conditions (4) are applied on both surfaces. The interactions remain weak, however, unless the rods approach to within a few diameters at some point along their axes, an unlikely prospect when $nl^3 \ll l/a$. Hence at dilute concentrations the effect on the velocities and the induced dipole is $O(\epsilon)$ smaller than the corresponding values for the isolated rod and can be calculated directly from (1) by using the disturbance velocity due to the second rod (as if isolated) in place of $\boldsymbol{u}_0$. The exact result, correct to first order in $\epsilon$ for separations of $O(1)$, is a complex function of the orientations, $\boldsymbol{q}_1$ and $\boldsymbol{q}_2$, and the relative position $\boldsymbol{R}$ (Berry 1982). Below we seek only the simpler far-field form.

Figure 1 illustrates the geometry of the interaction with $\boldsymbol{r} = s_1\boldsymbol{q}_1 + \boldsymbol{R} - s_2\boldsymbol{q}_2$ representing the vector between two arbitrary points on the rod axes. The rotational velocity of rod 1 in the presence of 2 is

$$\dot{\boldsymbol{q}}_1 = \dot{\boldsymbol{q}}_{10} + \frac{3}{2}\int_{-1}^{1} s_1(\boldsymbol{u}_2' - (\boldsymbol{u}_2'\cdot\boldsymbol{q}_1)\boldsymbol{q}_1)\,\mathrm{d}s_1, \tag{7}$$

with $\dot{\boldsymbol{q}}_{10}$ referring to an isolated rod and $\boldsymbol{u}_2'$ given by the integral in (1). In the far field

$$\boldsymbol{u}_2' = \boldsymbol{u}_2'(\boldsymbol{R}) + s_1\boldsymbol{q}_1\cdot\nabla\boldsymbol{u}_2'(\boldsymbol{R}) + \tfrac{1}{2}s_1^2\boldsymbol{q}_1\boldsymbol{q}_1 : \nabla\nabla\boldsymbol{u}_2'(\boldsymbol{R})$$

so that

$$\dot{\boldsymbol{q}}_1 = \dot{\boldsymbol{q}}_{10} + \boldsymbol{q}_1\cdot\nabla\boldsymbol{u}_2'(\boldsymbol{R})\cdot(\boldsymbol{\delta} - \boldsymbol{q}_1\boldsymbol{q}_1). \tag{8}$$

Similarly,

$$\begin{aligned}\boldsymbol{S}_{12} &= \boldsymbol{S}_{10} + \tfrac{1}{2}\boldsymbol{q}_1\boldsymbol{q}_1\boldsymbol{q}_1\cdot\boldsymbol{e}_2(\boldsymbol{R})\cdot\boldsymbol{q}_1 \\ &\equiv \boldsymbol{S}_{10} + \boldsymbol{S}_{12}',\end{aligned} \tag{9}$$

with $\boldsymbol{e}_2 = \frac{1}{2}(\nabla\boldsymbol{u}_2' + (\nabla\boldsymbol{u}_2')^{\mathrm{T}})$ and $\boldsymbol{S}_{10}$ the dipole for an isolated rod. The fact that the effect of the interaction is $O(\epsilon)$ smaller than the corresponding term for the isolated rod is evident from the scaling of $f$.

In the following sections we assimilate these results for the dynamics into a conservation equation for the suspension microstructure and an expression for the bulk stress which recognize far-field interactions among the rods.

## 3. Pre-averaged pair conservation equation

The probability density $P_N$ of a configuration of $N$ rods in a volume $V$ is defined by the $N$ generalized configuration space vectors $\boldsymbol{v}_i$ describing their positions and orientations. The resulting conservation equation,

$$\frac{\partial P_N}{\partial t}+\sum_i \nabla_{\boldsymbol{v}_i}\cdot\dot{\boldsymbol{v}}_i P_N = 0, \tag{10}$$

balances accumulation at a point in configuration space with generalized convection into the point. Denoting $\boldsymbol{C}_N = (\boldsymbol{v}_1, \ldots, \boldsymbol{v}_N)$ allows the normalizations for the probability density to be written as

$$\left.\begin{aligned} \int P_N \,\mathrm{d}\boldsymbol{C}_N &= N!, \\ \int P_N \,\mathrm{d}\boldsymbol{C}_{N-1} &= (N-1)!\,P_1 \\ \int P_N \,\mathrm{d}\boldsymbol{C}_{N-2} &= (N-2)!\,P_2, \end{aligned}\right\} \tag{11}$$

etc.

Since interactions are $O(\epsilon)$, the one- and two-particle probabilities can be expanded as

$$\left.\begin{aligned} P_1 &\equiv nl^3 f(\boldsymbol{q}_1), \\ P_2 &= n^2 l^6 f(\boldsymbol{q}_1) f(\boldsymbol{q}_2)(1+O(\epsilon)), \end{aligned}\right\} \tag{12}$$

with $f(\boldsymbol{q})\,\mathrm{d}\boldsymbol{q}$ the probability that an individual rod has orientation between $\boldsymbol{q}$ and $\boldsymbol{q}+\mathrm{d}\boldsymbol{q}$. Note that this expression for $P_2$ applies only for the accessible configurations; the probability density is zero for configurations that cause the rods to overlap.

An equation for $P_1$ or $f$, including the effects of pair interactions, can be derived by integrating the conservation equation (10) with respect to $\mathrm{d}\boldsymbol{C}_{N-1}$, i.e. over all configurational vectors but that describing rod 1. For $i \neq 1$

$$\int_V \nabla_{\boldsymbol{v}_i}\cdot\dot{\boldsymbol{v}}_i P_N \,\mathrm{d}\boldsymbol{C}_{N-1} = \int_A \boldsymbol{n}\cdot\dot{\boldsymbol{v}}_i P_N \,\mathrm{d}\boldsymbol{v}_i \,\mathrm{d}\boldsymbol{C}_{N-1} = 0, \tag{13}$$

with $A$ the surface enclosing $V$, since rods are conserved within the volume. This leaves

$$\frac{\partial P_1}{\partial t}+\frac{1}{(N-1)!}\int_{V_{\mathrm{acc}}} \nabla_{\boldsymbol{q}_1}\cdot\dot{\boldsymbol{q}}_1 P_N \,\mathrm{d}\boldsymbol{C}_{N-1} = 0, \tag{14}$$

with $V_{\mathrm{acc}}$ referring to the volume accessible to the rods. The integral in (14) can be decomposed into two terms representing the effect of the macroscopically imposed flow and the velocity disturbance $\boldsymbol{u}'_j$ produced by the presence of rod $j$. Then at steady state (14) reduces to

$$\nabla_{\boldsymbol{q}_1}\cdot\dot{\boldsymbol{q}}_{10} P_1 = -\frac{\epsilon}{(N-1)!}\sum_{j\neq 1} \nabla_{\boldsymbol{q}_1}\cdot\int \nabla_{\boldsymbol{r}_{1j}}\boldsymbol{u}'_j P_N \,\mathrm{d}\boldsymbol{C}_{N-1} : (\boldsymbol{q}_1\boldsymbol{\delta}-\boldsymbol{q}_1\boldsymbol{q}_1\boldsymbol{q}_1). \tag{15}$$

Unfortunately, $\nabla\boldsymbol{u}'_j$ decays as $R^{-3}$, making the integral in (15) conditionally convergent if evaluated directly. Hence, a renormalization akin to that developed by Batchelor & Green (1972) or Hinch (1977) for the bulk stress in a suspension of

spheres is necessary. Since the macroscopic velocity gradient is imposed on the suspension, the perturbations must integrate to zero as

$$\sum_{j=2}^{N} \int_V \nabla \boldsymbol{u}_j' P_{N-1} \, \mathrm{d}C_{N-1} = 0, \tag{16}$$

where $V$ includes both $V_{\mathrm{excl}}$, the volume excluded to one rod by the presence of a second, and $V_{\mathrm{acc}}$. Subtraction of a suitable multiple of (16) from (15) renders the integral convergent.

Since the other $N-1$ rods are indistinguishable, the renormalized ensemble average can be rewritten as

$$\nabla_{q_1} \cdot \dot{\boldsymbol{q}}_{10} P_1 = -\frac{\epsilon}{(N-2)!} \nabla_{q_1} \cdot \left\{ \int_{V_{\mathrm{acc}}} \nabla_{r_{12}} \boldsymbol{u}_2'(P_N - P_{N-1} nf(q_1)) \, \mathrm{d}C_{N-1} - \int_{V_{\mathrm{excl}}} \nabla_{r_{12}} \boldsymbol{u}_2' P_{N-1} nf(q_1) \, \mathrm{d}C_{N-1} \right\} : (\boldsymbol{q}_1 \boldsymbol{\delta} - \boldsymbol{q}_1 \boldsymbol{q}_1 \boldsymbol{q}_1). \tag{17}$$

Substitution of (11) and (12) into (17) demonstrates that $P_N = nfP_{N-1}(1+O(\epsilon))$, so the first integral is zero to order $\epsilon$.

Applying (12) and the divergence theorem then allows the conservation equation to be rewritten as

$$\nabla_{q_1} \cdot \dot{\boldsymbol{q}}_1 f(q_1) = O(\epsilon n^2 l^6), \tag{18}$$

with

$$\dot{\boldsymbol{q}}_1 = \dot{\boldsymbol{q}}_{10} - \tfrac{4}{3}\pi \epsilon n l^3 \{ \overline{\boldsymbol{\omega}} \cdot \boldsymbol{q}_1 + \overline{\boldsymbol{e}} : (\boldsymbol{q}_1 \boldsymbol{\delta} - \boldsymbol{q}_1 \boldsymbol{q}_1 \boldsymbol{q}_1) \}$$

and

$$\left.\begin{aligned} \overline{\boldsymbol{e}} &= \frac{1}{2} \int_{A_{\mathrm{excl}}} (\boldsymbol{n}\boldsymbol{u}_2' + \boldsymbol{u}_2' \boldsymbol{n}) f(q_2) \, \mathrm{d}^2\boldsymbol{R} \, \mathrm{d}\boldsymbol{q}_2, \\ \overline{\boldsymbol{\omega}} &= \frac{1}{2} \int_{A_{\mathrm{excl}}} (\boldsymbol{n}\boldsymbol{u}_2' - \boldsymbol{u}_2' \boldsymbol{n}) f(q_2) \, \mathrm{d}^2\boldsymbol{R} \, \mathrm{d}\boldsymbol{q}_2. \end{aligned}\right\} \tag{19}$$

Here $A_{\mathrm{excl}}$ refers to the surface of the excluded volume about rod 1 and $\boldsymbol{n}$ is the unit normal to that surface.

The rotational velocity $\dot{\boldsymbol{q}}_{10}$ includes the effect of the macroscopically applied flow field plus the motion arising from the Brownian torque,

$$\boldsymbol{T}^{\mathrm{Br}} = -Pe^{-1} \nabla_{q_1} \ln f(q_1), \tag{20}$$

produced by gradients in $f$. The linearity of the Stokes equation permits superposition of these effects as

$$\dot{\boldsymbol{q}}_{10} = \boldsymbol{\Omega} \cdot \boldsymbol{q}_1 + \boldsymbol{E} : (\boldsymbol{q}_1 \boldsymbol{\delta} - \boldsymbol{q}_1 \boldsymbol{q}_1 \boldsymbol{q}_1) - Pe^{-1} \nabla_{q_1} \ln f(q_1). \tag{21}$$

Substitution into (18) demonstrates that the hydrodynamic and Brownian dipoles produced by rod 2 create an augmented rate of strain ($\boldsymbol{E} - \frac{4}{3}\pi \epsilon n l^3 \overline{\boldsymbol{e}}$) and an augmented vorticity ($\boldsymbol{\Omega} - \frac{4}{3}\pi \epsilon n l^3 \overline{\boldsymbol{\omega}}$).

For far-field interactions, $\boldsymbol{u}_2'$ and $\boldsymbol{e}_2$ produced by rod 2 follow from (1), (6) and (9) as

$$\left.\begin{aligned} \boldsymbol{u}_2' &= -\tfrac{1}{3}(\boldsymbol{S}_{20}^{\mathrm{hyd}} + Pe^{-1} \boldsymbol{S}_{20}^{\mathrm{Br}}) : \left\{ \frac{-\boldsymbol{\delta R}}{3R^3} + \frac{\boldsymbol{RRR}}{R^5} \right\} + \frac{1}{3Pe} \left\{ \frac{\boldsymbol{R} \cdot \boldsymbol{S}_{20}^{\mathrm{Br}} - \boldsymbol{S}_{20}^{\mathrm{Br}} \cdot \boldsymbol{R}}{R^3} \right\} + O(R^{-3}) \\ \boldsymbol{e}_2 &= -(\boldsymbol{S}_{20}^{\mathrm{hyd}} + Pe^{-1} \boldsymbol{S}_{20}^{\mathrm{Br}}) : \left\{ \frac{\boldsymbol{\delta RR} + 2\boldsymbol{R\delta R} + \boldsymbol{RR\delta}}{R^5} - \frac{5\boldsymbol{RRRR}}{R^7} \right\} + O(R^{-4}), \end{aligned}\right\} \tag{22}$$

with

$$\boldsymbol{S}_{20}^{\mathrm{hyd}} = \tfrac{1}{2} \boldsymbol{q}_2 \cdot \boldsymbol{E} \cdot \boldsymbol{q}_2 \boldsymbol{q}_2 \boldsymbol{q}_2$$

and

$$\boldsymbol{S}_{20}^{\mathrm{Br}} = \tfrac{1}{2} \boldsymbol{q}_2 \nabla_{q_2} \ln f(q_2).$$

The symmetric hydrodynamic dipole $\boldsymbol{S}_{20}^{\mathrm{hyd}}$ generates no vorticity to accompany $\boldsymbol{e}_2$, but the Brownian dipole $\boldsymbol{S}_{20}^{\mathrm{Br}}$ does.

The conservation equation (18) describing the rod orientation probability $f$ contains the pre-averaged values, $\bar{\boldsymbol{e}}$ and $\bar{\boldsymbol{\omega}}$, obtained by integration over the orientation $\boldsymbol{q}_2$. Use of the identity

$$\nabla_q(f\boldsymbol{q}) = (\nabla_q f)\,\boldsymbol{q} + f(\boldsymbol{\delta} - \boldsymbol{qq}) \tag{23}$$

and Green's theorem for a closed spherical surface,

$$\int \nabla_q(f\boldsymbol{q})\,\mathrm{d}^2\boldsymbol{q} = 2\int \boldsymbol{qq}f\,\mathrm{d}^2\boldsymbol{q},$$

demonstrates that $\bar{\boldsymbol{S}}_{20}^{\mathrm{Br}}$ is symmetric so that

$$\bar{\boldsymbol{\omega}} = 0.$$

Calculation of $\bar{\boldsymbol{e}}$ requires the rod orientation function and the excluded-volume shape (§4).

The conservation equation (18) is linear in $f$ but contains coefficients that depend on all seven independent variables. Here we develop solutions via a double perturbation expansion with the first expansion in $\epsilon \ll 1$ as

$$f = (f^{(0)} - \tfrac{4}{3}\pi\epsilon n l^3 f^{(1)} + \ldots)(1 + O(\epsilon)). \tag{24}$$

Substitution into the steady-state conservation equation then decouples the $O(1)$ component

$$\nabla_{q_1}^2 f^{(0)}(\boldsymbol{q}_1) = Pe\,\nabla_{q_1}\cdot((\boldsymbol{\Omega} + \boldsymbol{E})\cdot\boldsymbol{q}_1 - \boldsymbol{q}_1\cdot\boldsymbol{E}\cdot\boldsymbol{q}_1\,\boldsymbol{q}_1) f^{(0)}(\boldsymbol{q}_1)$$

from the $O(\epsilon)$

$$\begin{aligned}\nabla_{q_1}^2 f^{(1)}(\boldsymbol{q}_1) = Pe\{&\nabla_{q_1}\cdot((\boldsymbol{\Omega}\cdot\boldsymbol{q}_1 + \boldsymbol{E}\cdot\boldsymbol{q}_1 - \boldsymbol{q}_1\cdot\boldsymbol{E}\cdot\boldsymbol{q}_1\,\boldsymbol{q}_1) f^{(1)}(\boldsymbol{q}_1)) \\ &+ \nabla_{q_1}\cdot((\bar{\boldsymbol{e}}\cdot\boldsymbol{q}_1 - \boldsymbol{q}_1\cdot\bar{\boldsymbol{e}}\cdot\boldsymbol{q}_1\,\boldsymbol{q}_1\,\boldsymbol{q}_1) f^{(0)}(\boldsymbol{q}_1))\},\end{aligned} \tag{25}$$

with $$\int f^{(0)}(\boldsymbol{q}_1)\,\mathrm{d}\boldsymbol{q}_1 = 1$$

and $$\int f^{(1)}(\boldsymbol{q}_1)\,\mathrm{d}\boldsymbol{q}_1 = 0.$$

The second expansion for $Pe \ll 1$

$$\left.\begin{aligned} f^{(0)} &= \frac{1}{4\pi}(1 + Pe\,f_1^{(0)} + Pe^2 f_2^{(0)} + Pe^3 f_3^{(0)} + \ldots), \\ f^{(1)} &= \frac{1}{4\pi}(Pe\,f_1^{(1)} + Pe^2 f_2^{(1)} + Pe^3 f_3^{(1)} + \ldots) \end{aligned}\right\} \tag{26}$$

then provides a hierarchy of equations for the $f_i^{(0)}$ and $f_i^{(1)}$. The results for isolated rods, summarized by Brenner (1974), are

$$\left.\begin{aligned} f_1^{(0)} &= \tfrac{1}{2}\boldsymbol{q}_1\cdot\boldsymbol{E}\cdot\boldsymbol{q}_1, \\ f_2^{(0)} &= \tfrac{1}{2}f_1^{(0)2} - \tfrac{1}{60}\,\mathrm{tr}\,(\boldsymbol{E}^2) - \tfrac{1}{12}\boldsymbol{q}_1\cdot\boldsymbol{J}(\boldsymbol{E})\cdot\boldsymbol{q}_1, \\ f_3^{(0)} &= f_1^{(0)} f_2^{(0)} - \tfrac{1}{3}f_1^{(0)3} + \tfrac{1}{60}f_1^{(0)}\boldsymbol{q}_1\cdot\boldsymbol{J}(\boldsymbol{E})\cdot\boldsymbol{q}_1 - \tfrac{1}{120}\boldsymbol{q}_1\cdot\boldsymbol{J}(\boldsymbol{E}^2)\cdot\boldsymbol{q}_1 + \tfrac{1}{72}\boldsymbol{q}_1\cdot\boldsymbol{J}^2(\boldsymbol{E})\cdot\boldsymbol{q}_1 - \tfrac{1}{630}\,\mathrm{tr}\,(\boldsymbol{E}^3). \end{aligned}\right\} \tag{27}$$

Here

$$\left.\begin{aligned} \boldsymbol{D}^n &= \boldsymbol{D}\cdot\boldsymbol{D}\cdot\ldots\cdot\boldsymbol{D}\,(n \text{ times}), \\ \mathrm{tr}\,(\boldsymbol{D}) &= \boldsymbol{\delta}:\boldsymbol{D}, \\ J(\boldsymbol{D}) &= \boldsymbol{D}\cdot\boldsymbol{\Omega} - \boldsymbol{\Omega}\cdot\boldsymbol{D}, \end{aligned}\right\} \tag{28}$$

the last being the steady-state form of the Jaumann derivative.

The second moment of the distribution function

$$\langle \boldsymbol{q}_1 \boldsymbol{q}_1 \rangle = \int \boldsymbol{q}_1 \boldsymbol{q}_1 f^{(0)}(\boldsymbol{q}_1)\, \mathrm{d}\boldsymbol{q}_1, \tag{29}$$

reflects the effect of flow on the orientation (Brenner 1974). For a simple shear flow with $E_{12} = E_{21} = \Omega_{12} = -\Omega_{21} = 1/\sqrt{2}$ the projection of the rod on the axis in the direction of flow is

$$\langle q_{1x} q_{1x} \rangle = \frac{1}{3}\left(1 + \frac{2Pe^2}{105}\right). \tag{30}$$

Hence the shear tends to align the rod.

The hierarchy of equations for $f_i^{(1)}$ now follow from substitution of (26) and (27) into (25) with

$$\begin{aligned} \bar{\boldsymbol{e}} &= \bar{\boldsymbol{e}}^{\mathrm{hyd}} + Pe^{-1}\bar{\boldsymbol{e}}^{\mathrm{Br}} \\ &= \bar{\boldsymbol{e}}_0 + Pe\,\bar{\boldsymbol{e}}_1 + Pe^2\bar{\boldsymbol{e}}_2 + \ldots \end{aligned} \tag{31}$$

(Berry 1982). In each $\nabla^2_{\boldsymbol{q}_1}$ operates on $f_i^{(1)}$, representing the effort of rotary diffusion to randomize the distribution, while the forcing terms arise from the strain fields $\bar{\boldsymbol{e}}_{i-1}$ acting on the isolated rods with $f_{i-1}^{(0)}(\boldsymbol{q}_1)$ and the applied field $\boldsymbol{E}+\boldsymbol{\Omega}$ acting on the lower-order $f_i^{(1)}$. Solution of these inhomogeneous equations produces

$$\left.\begin{aligned} f_1^{(1)} &= \tfrac{1}{2}\bar{e}_0, \\ f_2^{(1)} &= \tfrac{1}{4}E\bar{e}_0 - \tfrac{1}{30}\boldsymbol{E}:\bar{\boldsymbol{e}}_0 - \tfrac{1}{12}\boldsymbol{q}_1\cdot\boldsymbol{J}(\bar{\boldsymbol{e}}_0)\cdot\boldsymbol{q}_1 + \tfrac{1}{2}\bar{e}_1, \\ f_3^{(1)} &= \tfrac{1}{16}E^2\bar{e}_0 - \tfrac{1}{60}E\boldsymbol{E}:\bar{\boldsymbol{e}}_0 - \tfrac{1}{120}\boldsymbol{E}:\boldsymbol{E}\bar{e}_0 - \tfrac{1}{210}\boldsymbol{E}^2:\bar{\boldsymbol{e}}_0 \\ &\quad - \tfrac{1}{30}E\boldsymbol{q}_1\cdot\boldsymbol{J}(\bar{\boldsymbol{e}}_0)\cdot\boldsymbol{q}_1 - \tfrac{1}{30}\bar{e}_0\,\boldsymbol{q}_1\cdot\boldsymbol{J}(\boldsymbol{E})\cdot\boldsymbol{q}_1 - \tfrac{1}{60}\boldsymbol{q}_1\cdot\boldsymbol{J}(\boldsymbol{E}\cdot\bar{\boldsymbol{e}}_0)\cdot\boldsymbol{q}_1 \\ &\quad + \tfrac{1}{72}\boldsymbol{q}_1\cdot\boldsymbol{J}^2(\bar{\boldsymbol{e}}_0)\cdot\boldsymbol{q}_1 + \tfrac{1}{4}E\bar{e}_1 - \tfrac{1}{30}\boldsymbol{E}:\bar{\boldsymbol{e}}_1 - \tfrac{1}{12}\boldsymbol{q}_1\cdot\boldsymbol{J}(\bar{\boldsymbol{e}}_1)\cdot\boldsymbol{q}_1 + \tfrac{1}{2}\bar{e}_2, \end{aligned}\right\} \tag{32}$$

where

$$E = \boldsymbol{q}_1\cdot\boldsymbol{E}\cdot\boldsymbol{q}_1, \quad \bar{e}_i = \boldsymbol{q}_1\cdot\bar{\boldsymbol{e}}_i\cdot\boldsymbol{q}_1.$$

Explicit evaluation of these solutions requires substitution of the $f_i^{(0)}$ and integration. The hydrodynamic contribution to the rate of strain contains the fourth moment of $\boldsymbol{q}_2$ which can be reduced to second moments by multiplying the conservation equation for the isolated rod (25) by $\boldsymbol{q}_2\boldsymbol{q}_2\,\mathrm{d}^2\boldsymbol{q}_2$ and integrating (Brenner & Condiff 1974). The Brownian terms that contain the gradient of $f^{(0)}$ are reduced to second moments through (23). The result is

$$\begin{aligned} \bar{\boldsymbol{e}} = \frac{3}{16\pi}\int_{A_{\mathrm{excl}}} &\{[(\boldsymbol{E}+\boldsymbol{\Omega})\cdot\boldsymbol{q}_2\boldsymbol{q}_2 + \boldsymbol{q}_2\boldsymbol{q}_2\cdot(\boldsymbol{E}-\boldsymbol{\Omega}) - \tfrac{2}{3}\boldsymbol{E}:\boldsymbol{q}_2\boldsymbol{q}_2\boldsymbol{\delta}] \\ &+ 6Pe^{-1}(\boldsymbol{q}_2\boldsymbol{q}_2 - \tfrac{1}{3}\boldsymbol{\delta})\}:\frac{\boldsymbol{n}_0\boldsymbol{n}_0}{R^2}(\boldsymbol{n}_0\boldsymbol{n} + \boldsymbol{n}\boldsymbol{n}_0) f_0(\boldsymbol{q}_2)\,\mathrm{d}^2R\,\mathrm{d}\boldsymbol{q}_2 \end{aligned} \tag{33}$$

with $\boldsymbol{n}_0 = \boldsymbol{R}/R$.

To this point the analysis depends only on the asymptotic approximations for small $\epsilon$, $\phi$ and $Pe$ and the far-field form for $\boldsymbol{u}_2'$. The next section derives the unit normal $\boldsymbol{n}$ to the surface enclosing the excluded volume required for the evaluation of $\bar{\boldsymbol{e}}$.

## 4. Evaluation of the rate-of-strain disturbance for interacting rods

For hard, i.e. impenetrable, rods the excluded volume depends on the rod orientations as shown in figure 1. This rectangular parallelepiped, with volume $16al^2\sin\alpha$, forms a difficult, non-conformal geometry for evaluating $\boldsymbol{e}$ from (19). In

order to proceed analytically, we approximate the parallelepiped by an ellipsoid with equal volume and axis ratios. Then we define a pre-averaged excluded volume by averaging the moment of inertia of this ellipsoid over all orientations as

$$\langle \boldsymbol{I} \rangle = \int \boldsymbol{I}(\boldsymbol{q}_1 \boldsymbol{q}_2) f^{(0)}(\boldsymbol{q}_1) f^{(0)}(\boldsymbol{q}_2)\, \mathrm{d}\boldsymbol{q}_1\, \mathrm{d}\boldsymbol{q}_2. \tag{34}$$

With no imposed flow, the pre-averaged excluded volume reduces to a sphere. Weak flow fields ($Pe \ll 1$) deform the sphere slightly into an ellipsoid. This representation of the excluded volume, while *ad hoc*, is straightforward and should introduce no greater error than our far-field approximations for interactions.

The ellipsoid approximating the parallelepiped in figure 1 has basis vectors

$$\left.\begin{aligned} \boldsymbol{e}_b &= \frac{\boldsymbol{q}_1+\boldsymbol{q}_2}{[2(1+t)]^{\frac{1}{2}}}, \\ \boldsymbol{e}_c &= \frac{\boldsymbol{q}_1-\boldsymbol{q}_2}{[2(1-t)]^{\frac{1}{2}}}, \\ \text{and} \qquad \boldsymbol{e}_d &= \frac{\boldsymbol{q}_1 \times \boldsymbol{q}_2}{S}, \end{aligned}\right\} \tag{35}$$

where $S = |\boldsymbol{q}_1 \times \boldsymbol{q}_2| = \sin\alpha$ and $t = \boldsymbol{q}_1 \cdot \boldsymbol{q}_2 = \cos\alpha$. The semiaxis lengths $b$, $c$ and $d$ are found by equating the volumes,

$$\frac{4\pi}{3} bcd = 16 a l^3 S,$$

and the axis ratios

$$\frac{b}{c} = \left(\frac{1+t}{1-t}\right)^{\frac{1}{2}}$$

$$\frac{d}{b} = \frac{a\sqrt{2}}{l(1+t)^{\frac{1}{2}}},$$

of the parallelepiped and equivalent ellipsoid. The result is

$$\left.\begin{aligned} b &= 1.393 l(1+t)^{\frac{1}{2}}, \\ c &= 1.393 l(1-t)^{\frac{1}{2}}, \\ d &= 1.970 a. \end{aligned}\right\} \tag{36}$$

The moment of inertia for this ellipsoid is

$$\boldsymbol{I} = \frac{4\pi}{15} bcd[(c^2+d^2)\,\boldsymbol{e}_b \boldsymbol{e}_b + (b^2+d^2)\,\boldsymbol{e}_c \boldsymbol{e}_c + (b^2+c^2)\,\boldsymbol{e}_d \boldsymbol{e}_d]. \tag{37}$$

To pre-average we substitute $f^{(0)}$ from (26) and $\boldsymbol{I}$ from (37) into (34), and then evaluate the integral by expressing $\boldsymbol{q}_2$ in terms of a system of basis vectors containing $\boldsymbol{q}_1$ (see the Appendix) and using the orthogonality relationships (i.e. $\int \boldsymbol{q}\boldsymbol{q}\, \mathrm{d}^2\boldsymbol{q} = \frac{4}{3}\pi\boldsymbol{\delta}$, etc.). This ultimately produces

$$\langle \boldsymbol{I} \rangle = 7.414 \frac{4\pi^2}{45} a l^4 \left\{ \boldsymbol{\delta} - \tfrac{7}{80} Pe\, \boldsymbol{E} + \frac{Pe^2}{3360}[-30\boldsymbol{E}^2 - 4\boldsymbol{E}^2 : \boldsymbol{\delta}\boldsymbol{\delta} + 49 \boldsymbol{J}(\boldsymbol{E})] \right\} \tag{38}$$

for a linear shear flow. In the absence of flow, the suspension is isotropic and (38) reduces to

$$\langle \boldsymbol{I} \rangle = 6.504 a l^4 \boldsymbol{\delta}, \tag{39}$$

corresponding to a sphere of radius $r_0 = 1.312(a l^4)^{\frac{1}{5}}$. With flow the anisotropy of $\boldsymbol{I}$ reflects the structure induced in the suspension.

To determine the unit normal $\boldsymbol{n}$ we write the general equation for an ellipsoid as

$$1 = r^2 \boldsymbol{n}_0 \cdot \boldsymbol{A} \cdot \boldsymbol{n}_0 \tag{40}$$

where $r$, the distance from the centre of the ellipsoid to a point on the surface, is scaled on the characteristic length $r_0$ and $\boldsymbol{n}_0 = \boldsymbol{r}/r$. Since the excluded volume differs only slightly from a sphere $A$ and $r$ can be expanded as

$$\left.\begin{aligned} \boldsymbol{A} &= \boldsymbol{\delta} + Pe\,\boldsymbol{A}_1 + Pe^2 \boldsymbol{A}_2 + \ldots, \\ r^2 &= 1 + Pe\,a_1 + Pe^2 a_2 + \ldots, \end{aligned}\right\} \tag{41}$$

which produces

$$\begin{aligned} a_1 &= -\boldsymbol{n}_0 \cdot \boldsymbol{A}_1 \cdot \boldsymbol{n}_0, \\ a_2 &= -\boldsymbol{n}_0 \cdot \boldsymbol{A}_2 \cdot \boldsymbol{n}_0 + (\boldsymbol{n}_0 \cdot \boldsymbol{A}_1 \cdot \boldsymbol{n}_0)^2. \end{aligned}$$

The normal then is found from

$$\boldsymbol{n} = \frac{\nabla F}{(\nabla F \cdot \nabla F)^{\frac{1}{2}}} \tag{42}$$

with

$$F = r - [1 + Pe\,a_1 + Pe^2 a_2 + \ldots]^{\frac{1}{2}} = 0$$

so that

$$\begin{aligned} \boldsymbol{n} = \boldsymbol{n}_0 + Pe[\boldsymbol{A}_1 \cdot \boldsymbol{n}_0 - \boldsymbol{n}_0 \cdot \boldsymbol{A}_1 \cdot \boldsymbol{n}_0 \boldsymbol{n}_0] + \tfrac{1}{2} Pe^2 [(2\boldsymbol{A}_2 - 2\boldsymbol{n}_0 \cdot \boldsymbol{A}_1 \cdot \boldsymbol{n}_0 \boldsymbol{A}_1) \cdot \boldsymbol{n}_0 \\ - (2\boldsymbol{n}_0 \cdot \boldsymbol{A}_2 \cdot \boldsymbol{n}_0 - 3(\boldsymbol{n}_0 \cdot \boldsymbol{A}_1 \cdot \boldsymbol{n}_0)^2 + \boldsymbol{n}_0 \cdot \boldsymbol{A}_1^2 \cdot \boldsymbol{n}_0)\,\boldsymbol{n}_0]. \end{aligned} \tag{43}$$

Similarly, expanding the moment of inertia, scaled on $r_0^5$, as

$$\begin{aligned} \boldsymbol{I} &= \frac{1}{5} \int_A r^5 [\boldsymbol{n}_0 \cdot \boldsymbol{n} \boldsymbol{\delta} - \boldsymbol{n}_0 \boldsymbol{n}_0 \boldsymbol{n}_0 \cdot \boldsymbol{n}]\, \mathrm{d}a \\ &= \boldsymbol{I}_0 + Pe\,\boldsymbol{I}_1 + Pe^2 \boldsymbol{I}_2 + \ldots \end{aligned} \tag{44}$$

with

$$\mathrm{d}a = \left(1 + \frac{1}{r^2} \nabla_{\boldsymbol{n}_0} r \cdot \nabla_{\boldsymbol{n}_0} r\right)^{\frac{1}{2}} \mathrm{d}\boldsymbol{n}_0$$

and substituting (41) and (43) yields

$$\left.\begin{aligned} \boldsymbol{I}_0 &= \frac{8\pi}{15} \boldsymbol{\delta}, \\ \boldsymbol{I}_1 &= \frac{2\pi}{15} (\boldsymbol{A}_1 + \boldsymbol{A}_1^{\mathrm{T}} - 4\boldsymbol{A}_1 : \boldsymbol{\delta}\boldsymbol{\delta}), \\ \boldsymbol{I}_2 &= \frac{2\pi}{15} (\boldsymbol{A}_2 + \boldsymbol{A}_2^{\mathrm{T}} - 4\boldsymbol{A}_2 : \boldsymbol{\delta}\boldsymbol{\delta}) + \frac{2\pi}{525} [-64\boldsymbol{A}_1^2 + 89 A_1^2 : \boldsymbol{\delta}\boldsymbol{\delta}]. \end{aligned}\right\} \tag{45}$$

Matching with (38) then produces

$$\left.\begin{aligned} O(Pe) \quad & \boldsymbol{A}_1 = -\tfrac{7}{40} \boldsymbol{E} \\ O(Pe^2) \quad & \boldsymbol{A}_2 = \tfrac{1}{336\,000} [4290 \boldsymbol{E}^2 + 1531 \boldsymbol{E}^2 : \boldsymbol{\delta}\boldsymbol{\delta} + 9800 \boldsymbol{J}(\boldsymbol{E})]. \end{aligned}\right\} \tag{46}$$

Finally the unit normal takes the form

$$\begin{aligned} \boldsymbol{n} = \boldsymbol{n}_0 - \frac{7Pe}{40} (\boldsymbol{E} \cdot \boldsymbol{n}_0 - \boldsymbol{n}_0 \cdot \boldsymbol{E} \cdot \boldsymbol{n}_0 \boldsymbol{n}_0) - \frac{Pe^2}{67\,000} \{[858 \boldsymbol{E}^2 + 1960 \boldsymbol{J}(\boldsymbol{E}) - 2058 \boldsymbol{n}_0 \cdot \boldsymbol{E} \cdot \boldsymbol{n}_0 \boldsymbol{E}] \cdot \boldsymbol{n}_0 \\ - [1887 \boldsymbol{n}_0 \cdot \boldsymbol{E}^2 \cdot \boldsymbol{n}_0 + 1960 \boldsymbol{n}_0 \cdot \boldsymbol{J}(\boldsymbol{E}) \cdot \boldsymbol{n}_0 - 3087 (\boldsymbol{n}_0 \cdot \boldsymbol{E}_0 \cdot \boldsymbol{n})^2] \boldsymbol{n}_0\}. \end{aligned} \tag{47}$$

The expression for $\bar{\boldsymbol{e}}$, expanded for small $Pe$ in (31), can now be evaluated using the results for $\int \boldsymbol{q}_2\boldsymbol{q}_2 f^{(0)}\,\boldsymbol{q}_2$ found in Brenner (1974). Substitution of (4.7) into (3.3) and integration over $\boldsymbol{R}$ produces

$$\left.\begin{aligned}
\bar{\boldsymbol{e}}_0 &= \tfrac{8}{75}\boldsymbol{E}\\
\bar{\boldsymbol{e}}_1 &= \tfrac{1}{7875}[87\boldsymbol{E}^2 - 29\boldsymbol{E}^2{:}\boldsymbol{\delta}\boldsymbol{\delta} - 105\boldsymbol{J}(\boldsymbol{E})]\\
\bar{\boldsymbol{e}}_2 &= \tfrac{1}{13\,230\,000}[14\,190\boldsymbol{E}^3 - 4730\boldsymbol{E}^3{:}\boldsymbol{\delta}\boldsymbol{\delta} - 13\,453\boldsymbol{E}^2{:}\boldsymbol{\delta}\boldsymbol{E} - 30\,765\boldsymbol{J}(\boldsymbol{E}^2) + 29\,400\boldsymbol{J}^2(\boldsymbol{E})].
\end{aligned}\right\} \tag{48}$$

Note that the particle feels the enhanced rate of strain $\frac{4}{3}\pi l^3 \epsilon n \frac{8}{75}\boldsymbol{E}$ even though the excluded volume is $16\pi a l^2 n$. This occurs because the rate of strain near an isolated rod is $O(l/a)$.

These indicate that for a simple shear flow interactions affect the rod orientation at $O(Pe^2)$ as

$$\tfrac{4}{3}\pi\epsilon \iint \boldsymbol{q}_1\boldsymbol{q}_1 f^{(1)}\,\mathrm{d}\boldsymbol{q}_1\,\mathrm{d}\boldsymbol{R} = \frac{599\pi}{354\,375}\boldsymbol{E},$$

increasing the alignment in the direction of shear beyond that found at infinite dilution (30) due to the enhanced rate of strain in the fluid. With these results we can now proceed to evaluate the stresses.

## 5. The bulk stress for interacting rods

In a suspension of interacting rods a variety of processes contribute to the bulk stress. The first important distinction is between mechanical and thermodynamical, or direct Brownian, stresses. The latter arise from the increase in free energy due to the non-equilibrium state of the suspension, as reflected by the apparent thermodynamic torques cited in §3. The former include both hydrodynamic and indirect Brownian components, with the hydrodynamic deriving from the inability of the rod to deform with the fluid and the Brownian from the viscous stresses induced by particle rotations under the influence of the thermodynamic torques. Below we develop the bulk stress based on earlier work for isolated rods (Giesekus 1962) and interacting spheres (Batchelor & Green 1972; Batchelor 1977) but include the effect of interaction on the rod orientation.

### 5.1. *Hydrodynamic and Brownian contributions*

The general expression for the hydrodynamic contribution to the bulk stress is (Batchelor 1970*a*)

$$\boldsymbol{\Sigma} = -p\boldsymbol{\delta} + 2\boldsymbol{E} + \frac{8\pi\epsilon}{3V}\sum_{i=1}^{N}\boldsymbol{S}_i^{\mathrm{hyd}} \tag{49}$$

with $\boldsymbol{S}_i^{\mathrm{hyd}}$ representing the dipole induced in the $i$th rod by the local rate of strain. For pair interactions

$$\boldsymbol{S}_i^{\mathrm{hyd}} = \boldsymbol{S}_{i0}^{\mathrm{hyd}} + \epsilon\sum_{j+1}\boldsymbol{S}'_{ij}, \tag{50}$$

where $\boldsymbol{S}'_{ij}$ is calculated from (9) and (22) with $\boldsymbol{S}_{20}^{\mathrm{hyd}}$ replaced by $\boldsymbol{S}_{j0}^{\mathrm{hyd}} + Pe^{-1}\boldsymbol{S}_{j0}^{\mathrm{Br}}$. Conversion of the sums above to ensemble averages produces with (12) and (24)

$$\begin{aligned}
\boldsymbol{\Sigma} &= -p\boldsymbol{\delta} + 2\boldsymbol{E} + \frac{8\pi\epsilon n l^3}{3(N-1)!}\int\left(\boldsymbol{S}_{10}^{\mathrm{hyd}} + \epsilon\sum_{j-2}^{N}\boldsymbol{S}'_{ij}\right)P_N\,\mathrm{d}C_{N-1}\,\mathrm{d}\boldsymbol{q}_1\\
&= -p\boldsymbol{\delta} + 2\boldsymbol{E} + \tfrac{8}{3}\pi\epsilon n l^3\left\{\int \boldsymbol{S}_{10}^{\mathrm{hyd}} f^{(0)}\,\mathrm{d}\boldsymbol{q} - 4\pi\epsilon n l^3\int_{V_{\mathrm{excl}}}(\boldsymbol{S}_{10}^{\mathrm{hyd}} f^{(1)} + \bar{\boldsymbol{S}}' f^{(0)})\,\mathrm{d}\boldsymbol{q}_1 + O(nl^3\epsilon)^2\right\},
\end{aligned} \tag{51}$$

where $\bar{\boldsymbol{S}}' = \frac{1}{2}\boldsymbol{q}_1\boldsymbol{q}_1\boldsymbol{q}_1{\cdot}\bar{\boldsymbol{e}}{\cdot}\boldsymbol{q}_1$.

The first term comprises the single-particle contribution; interactions affect the stress at $O(nl^3)^2$ both by altering the orientation distribution function $f$ and by inducing an additional dipole $\boldsymbol{S}'$. Since $\overline{\boldsymbol{e}}$ decays as $R^{-3}$, the latter term has been renormalized with (16).

The Brownian stress $\boldsymbol{\tau}$ follows from (Giesekus 1962)

$$\frac{3}{8\pi\epsilon}\boldsymbol{\tau} = nl^3 Pe^{-1}\int \boldsymbol{q}\nabla_q f \,\mathrm{d}\boldsymbol{q} \tag{52}$$

and the expansion in (24). Combining the hydrodynamic and Brownian terms yields the complete bulk stress as

$$\boldsymbol{\Sigma}+\boldsymbol{\tau} = -p\boldsymbol{\delta}+2\boldsymbol{E}+\tfrac{8}{3}\pi\epsilon nl^3\left\{\int(\boldsymbol{S}_{10}^{\mathrm{hyd}}f^{(0)}+Pe^{-1}\boldsymbol{q}_1\nabla_{q_1}f^{(0)})\right.$$
$$\left.-4\pi\epsilon nl^3\int_{V_{\mathrm{excl}}}(\overline{\boldsymbol{S}}'f^{(0)}+\boldsymbol{S}_{10}^{\mathrm{hyd}}f^{(1)}+Pe^{-1}\boldsymbol{q}_1\nabla_{q_1}f^{(1)})\,\mathrm{d}\boldsymbol{q}_1\right\}. \tag{53}$$

### 5.2. *General results for* $Pe \ll 1$

Determination of the bulk stress requires evaluation of the second moment of $\boldsymbol{q}_1$. Brenner (1974) provides the $O(1)$ expression, while the $O(\epsilon)$ term is

$$\int \boldsymbol{q}_1\boldsymbol{q}_1 f^{(1)}\,\mathrm{d}\boldsymbol{q}_1 = \frac{Pe}{15}\overline{\boldsymbol{e}}_0+\frac{Pe^2}{630}[6(\boldsymbol{E}\cdot\overline{\boldsymbol{e}}_0+\overline{\boldsymbol{e}}_0\cdot\boldsymbol{E})-4(\boldsymbol{E}:\overline{\boldsymbol{e}}_0)\boldsymbol{\delta}-7\boldsymbol{J}(\overline{\boldsymbol{e}}_0)+42\overline{\boldsymbol{e}}_1]$$
$$+\frac{Pe^3}{18900}\{20(\boldsymbol{E}\cdot\boldsymbol{E}\cdot\overline{\boldsymbol{e}}_0+\overline{\boldsymbol{e}}_0\cdot\boldsymbol{E}\cdot\boldsymbol{E}+\boldsymbol{E}\cdot\overline{\boldsymbol{e}}_0\cdot\boldsymbol{E})-32(\boldsymbol{E}:\overline{\boldsymbol{e}}_0)\boldsymbol{E}-16(\boldsymbol{E}:\boldsymbol{E})\overline{\boldsymbol{e}}_0$$
$$-20(\boldsymbol{E}^2:\overline{\boldsymbol{e}}_0)\boldsymbol{\delta}-45[\boldsymbol{J}(\boldsymbol{E}\cdot\overline{\boldsymbol{e}}_0)+\boldsymbol{J}(\overline{\boldsymbol{e}}_0\cdot\boldsymbol{E})]+35\boldsymbol{J}^2(\overline{\boldsymbol{e}}_0)+180(\boldsymbol{E}\cdot\overline{\boldsymbol{e}}_1+\overline{\boldsymbol{e}}_1\cdot\boldsymbol{E})$$
$$-120(\boldsymbol{E}:\overline{\boldsymbol{e}}_1)\boldsymbol{\delta}-210\boldsymbol{J}(\overline{\boldsymbol{e}}_1)+1260\overline{\boldsymbol{e}}_2+630\overline{\boldsymbol{e}}_2:\boldsymbol{\delta}\boldsymbol{\delta}\}. \tag{54}$$

The final results, with isotropic terms suppressed, follow as

$$\boldsymbol{\Sigma}+\boldsymbol{\tau} = 2\boldsymbol{E}+\sum_{n=0}^{2}\sum_{m=1}^{2} Pe^n\left(\frac{16\pi l^3}{45}\epsilon n\right)^m \boldsymbol{\sigma}_{mn}, \tag{55}$$

with

$$\boldsymbol{\sigma}_{10} = 2\boldsymbol{E},$$
$$\boldsymbol{\sigma}_{11} = \tfrac{5}{14}\boldsymbol{E}^2-\tfrac{1}{4}\boldsymbol{J}(\boldsymbol{E}),$$
$$\boldsymbol{\sigma}_{12} = \tfrac{1}{21}\boldsymbol{E}^3-\tfrac{3}{140}\,\mathrm{tr}\,(\boldsymbol{E}^2)\boldsymbol{E}-\tfrac{11}{168}\boldsymbol{J}(\boldsymbol{E}^2)+\tfrac{1}{24}\boldsymbol{J}^2(\boldsymbol{E}),$$
$$\boldsymbol{\sigma}_{20} = \tfrac{4}{5}\boldsymbol{E},$$
$$\boldsymbol{\sigma}_{21} = \tfrac{129}{350}\boldsymbol{E}^2-\tfrac{1}{5}\boldsymbol{J}(\boldsymbol{E}),$$
$$\boldsymbol{\sigma}_{22} = \tfrac{5573}{58\,800}\boldsymbol{E}^3-\tfrac{33\,897}{784\,000}\boldsymbol{E}^2:\boldsymbol{\delta}\boldsymbol{E}-\tfrac{549}{5600}\boldsymbol{J}(\boldsymbol{E}^2)+\tfrac{11}{240}\boldsymbol{J}^2(\boldsymbol{E}).$$

The complexity of these expressions precludes any immediate conclusions beyond noting the zero shear viscosity to be

$$\mu\left[1+\frac{16\pi l^3}{45}\epsilon n+\frac{2}{5}\left(\frac{16\pi l^2}{45}\epsilon n\right)^2+O(nl^3)^3\right]. \tag{56}$$

The corresponding value of $\frac{2}{5}$ for the Huggins coefficient, characterizing the pair interactions, coincides with the values for porous spheres in the free-draining limit (Felderhof 1976; Russel 1979) or the far-field contribution for solid spheres (Batchelor

1977). For spheres, however, only hydrodynamic interactions enter, whereas with rods the Brownian torques provide a significant fraction (75%) of both the $O(nl^3)$ and the pair-interaction terms. Consequently, as we shall see more clearly in the next section, the Huggins coefficient varies with $Pe$ and type of flow, in contrast to the situation with spheres for which the far-field contribution remains Newtonian.

## 6. Viscometric functions for simple shear and steady elongation

These two flow fields illustrate somewhat better than the general equation (55) the consequences of pair interactions in a suspension of rods. The results for isolated rods are included for comparison.

For simple shear with $E_{12} = E_{21} = \Omega_{12} = -\Omega_{21} = 1/\sqrt{2}$, the relative viscosity

$$\bar{\mu} = \Sigma_{12}$$

and the two normal stress differences

$$N_1 = \Sigma_{11} - \Sigma_{22},$$
$$N_2 = \Sigma_{22} - \Sigma_{33}$$

fully describe the rheology. Here all quantities remain dimensionless as before, but the bulk stresses above include both the hydrodynamic and Brownian parts.

From (55) one finds

$$\bar{\mu} = 1 + [\eta]n + k[\eta]^2 n^2 + \ldots, \tag{57}$$

with

$$[\eta] = \frac{16\pi l^3}{45}\epsilon(1 - 0.020Pe^2 + \ldots),$$

$$k = \tfrac{2}{5}(1 - 0.0142Pe^2 + \ldots)$$

and

$$N_1 = Pe\frac{4\pi l^3}{45}\epsilon n\left(1 + 3.2\frac{4\pi l^3}{45}\epsilon n + \ldots\right),$$

$$N_2 = -\tfrac{1}{7}Pe\frac{4\pi l^3}{45}\epsilon n\left(1 + 0.88\frac{4\pi l^3}{45}\epsilon n + \ldots\right).$$

For each the interactions enhance the non-Newtonian effects predicted at infinite dilution.

At $O(n)$ alignment of the isolated rods by the shear flow decreases the shear stress and, hence, the effective hydrodynamic volume $[\eta]$. The shear thinning at $O(n^2)$ reflects this as well, but also includes a slightly larger effect on $k$, due to further alignment of the rods by hydrodynamic interactions. Although both normal stresses increase in absolute magnitude, the ratio

$$\frac{N_1}{N_2} = -\frac{1}{7}\left(1 - 2.32\frac{4\pi l^3}{45}\epsilon n + \ldots\right) \tag{58}$$

decreases.

Without the deformation of the excluded volume, (57) and (58) would be

$$k' = \tfrac{2}{5}(1 - 0.009Pe^2),$$

$$N_1' = Pe\frac{4\pi l^3}{45}\epsilon n\left(1 + 3.2\frac{4\pi l^3}{45}\epsilon n + \ldots\right),$$

$$N_2' = -\tfrac{1}{7}Pe\frac{4\pi l^3}{45}\epsilon n\left(1-0.8\frac{4\pi l^3}{45}\epsilon n+\ldots\right),$$

$$\frac{N_2'}{N_1'} = -\frac{1}{7}\left(1-4.0\frac{4\pi l^3}{45}\epsilon n+\ldots\right).$$

Consequently, the effect of alignment on the excluded volume significantly alters the rheology, enhancing the shear thinning of the viscosity and the second normal stress, but leaving the first normal stress unchanged.

For axisymmetric extension with $E_{11} = -2E_{22} = -2E_{33} = \sqrt{6}/3$ and $\Omega_{ij} = 0$ the Trouton viscosity

$$\begin{aligned}\bar{\eta}_{\mathrm{T}} &= \tfrac{1}{2}\sqrt{6}[\Sigma_{11}-\tfrac{1}{2}(\Sigma_{22}+\Sigma_{33})]\\ &= 3(1+[\eta_{\mathrm{T}}]n+k_{\mathrm{T}}[\eta_{\mathrm{T}}]^2n^2+\ldots)\end{aligned} \tag{59}$$

characterizes the fluid response. From (52)

$$\left.\begin{aligned}[\eta_{\mathrm{T}}] &= \frac{16\pi l^3}{45}\epsilon(1+\tfrac{5}{56}Pe+\tfrac{1}{560}Pe^2+\ldots),\\ k_{\mathrm{T}} &= \tfrac{2}{5}(1+0.0518Pe-0.0130Pe^2+\ldots).\end{aligned}\right\} \tag{60}$$

Here again increased alignment with the direction of the flow produces a larger stress. However, $[\eta_{\mathrm{T}}]$ grows somewhat faster than $k_{\mathrm{T}}$.

For a spherical excluded volume (60) becomes

$$k_{\mathrm{T}}' = \tfrac{2}{5}[1+0.0893Pe-0.0044Pe^2],$$

indicating again that alignment decreases the interactions between the rods.

These two examples illustrate the overall influence of interactions on the rheology of concentrated suspensions of rods. In both cases the $O(n^2)$ terms increase the non-Newtonian effects expected at infinite dilution. The predictions remain in qualitative accord with dilute theories but the $O(n^2)$ corrections portend important quantitative effects of interactions at higher concentrations. In this sense this theory, valid for $nl^3\epsilon < 1$, provides a bridge from the dilute $nl^3\epsilon \ll 1$ to the semi-dilute $nl^3 \gg 1$ regimes. We will pursue this point further after juxtaposing the predictions with data for a semi-rigid macromolecule.

## 7. Comparison with experimental results

The literature contains little or no data on the concentration dependence of the viscometric functions for dilute suspensions of truly rigid rods without electroviscous effects. However, Xanthan gum, with molecular weights of $\approx 10^6$–$10^7$, at moderately high salt concentrations ($\approx$0.1 M NaCl) apparently behave somewhat like a rigid, uncharged rod. Although the macromolecule carries some fixed charges and retains some flexibility (Holzwarth 1978), Whitcomb & Macosko (1978) successfully fit their shear-thinning intrinsic-viscosity data via the rigid-rod theory. Here we use the more complete data of Chauveteau (1982) which reveals the shear-rate dependence of both the intrinsic viscosity and the Huggins coefficient.

When expressed in terms of the weight concentration, the theory contains three parameters: $a$, $l$ and $M$ (the molecular weight). The data for the intrinsic viscosity readily yield a value for the low-shear limit $[\eta]_0$ and, from the shear-thinning behaviour, the rotary diffusion coefficient $D_0$. From the theory

$$M = \frac{2}{15}\frac{kT}{\mu}\frac{N_{\mathrm{A}}}{[\eta]_0 D_0},$$

| Batch | $[\eta]_0$ | $D_0$ | $M$ | $2l$ | $m$ |
|---|---|---|---|---|---|
| A | 4.3 m³/kg | 133 s⁻¹ | 587 kg/mole | 0.58 μm | 1.01 kg/nm-mole |
| B | 3.9 | 109 | 700 | 0.62 | 1.27 |

TABLE 1. Values extracted from the data and results of Chauveteau (1982)

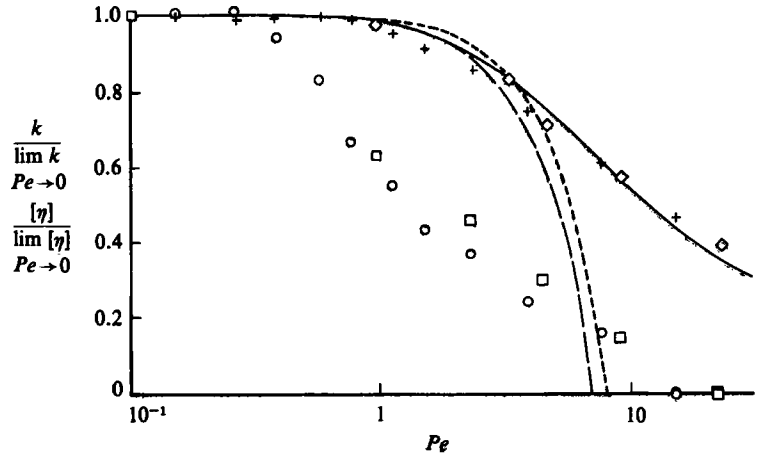


FIGURE 2. Data from Chauveteau (1982) for dilute solutions of Xanthan gum in 0.1 M NaCl;

| batch | | $[\eta]$ | $k$ |
|---|---|---|---|
| A | data | + | ○ |
| | $\lim Pe\to 0$ | 4.3 m³/kg | 0.454 |
| B | data | ◇ | □ |
| | $\lim Pe\to 0$ | 3.9 m³/kg | 0.455 |

Theory: ——, numerical results for $[\eta]$ (Scheraga 1955); ———, $O(Pe^2)$ expansion for $[\eta]$ (Hinch & Leal 1972); – – – –, $O(Pe^2)$ expansion for $k$ (equation 55).

where $N_A$ = Avogadro's number. For a single-stranded Xanthan gum $a \approx 1.0$ nm (Holzwarth & Prestridge 1978). Finally the length follows from the measured $[\eta]_0$ and the theoretical result

$$[\eta]_0 = \frac{16\pi}{45}\frac{N_A l^3}{M \ln 2l/a}.$$

Table 1 summarizes the values extracted from the data for $[\eta]_0$ and $D_0$ and the results for $M$, $l$ and $m = M/2l$. The last fall close to that deduced for a single strand from the molecular structure of Xanthan, 0.93 kg/nm-mole, but the first lie well below the molecular weights from light scattering reported by Chauveteau (1982).

Figure 2 shows our fit of the $O(n)$ theory to Chauveteau's (1982) measurements for two slightly different molecular weights at 0.1 M NaCl. The shear-rate dependence of $[\eta]$ conforms to the predictions from the numerical solutions of Scheraga (1955) (see Brenner 1974) over the entire range of shear rates, lending some credibility to the rigid-rod model despite the discrepancy in molecular weights.

Figure 2 also compares our $O(Pe^2)$ theory for $k$ with the measured values. The low-shear limit (0.45) exceeds slightly the predicted value (0.40). The shear-rate dependence, however, significantly exceeds that predicted for $Pe \leqslant 1$. These discre-

pancies may reflect the two approximations in the theory, the far-field form for the interactions and the representation of the excluded volume by an equivalent ellipsoid, or merely that these Xanthan gum suspensions are not a good model system for rigid-rod interactions.

## 8. Relationship to semi-dilute theories

At concentrations beyond the dilute regime near-field hydrodynamic interactions among many rods become important. Two approximate approaches propose reasonable alternatives to the intractable many-body problems that an exact theory would have to confront. Both apply to the semi-dilute regime for which $1 \ll l^3n \ll (l/a)^2$.

The first, due to Batchelor (1971), pertains to extensional flow, which aligns all rods in the direction of extension in the $Pe \to \infty$ limit. With slender-body theory and the idea that neighbouring rods, in effect, form a cell of radius $r = (2\pi ln)^{-\frac{1}{2}}$ about the test rod, he derived the extensional viscosity as

$$\bar{\eta}_T = 3\left(1 + \frac{4\pi}{9}\frac{l^3n}{\ln r/a}\right). \tag{61}$$

The logarithmic dependence on $r$ obviates the uncertainty in defining the cell. As noted later (Batchelor 1976), the results of this theory, which remain valid for $\bar{\eta}_T \gg 3$, agree quite satisfactorily with experimental data. Since extension of our theory to $Pe \gg 1$ remains to be done, we cannot comment on the transition from dilute to semi-dilute behaviour in this case.

The recent theory of Doi & Edwards (1978*a*, *b*) addresses conditions more compatible with our work. They propose a means for correcting the rotary diffusion coefficient of a particular rod for the effects of interactions with many neighbours at semi-dilute concentrations. The authors ignore weak far-field interactions, but consider the 'constraints' that prevent rods from passing through one another while rotating or translating perpendicular to their axes. Either lubrication stresses, associated with near-field hydrodynamic interactions between rods having diameters large relative to the solvent molecules, or repulsive interaction potentials between the rods themselves would provide the necessary forces. From geometrical arguments they deduce the effective rotary diffusion coefficient to be

$$\frac{\beta D_0}{(8nl^3)^2}$$

at equilibrium, with an additional correction due to alignment at higher shear rates. $\beta$ is an unknown constant assumed to be $O(1)$.

The calculations of the orientation distribution function and the particle stress then proceed much as in the dilute limit, although some ambiguity remains concerning the appropriate diffusivity to be used in the latter (Jain & Cohen 1981). For $Pe \ll 1$ Doi & Edwards (1978*b*) obtained

$$\left.\begin{aligned} \bar{\mu} &= \frac{36}{5\pi^2\beta\epsilon^2}\left(\frac{4\pi}{3}\epsilon nl^3\right)^3 + O(Pe^2), \\ N_1 &= -\tfrac{7}{2}N_2 = \frac{144}{5\pi^4(\beta\epsilon^2)^2}\left(\frac{4\pi}{3}\epsilon nl^3\right)^4 Pe. \end{aligned}\right\} \tag{62}$$

Figures 3 and 4 compare the predictions of the two theories.

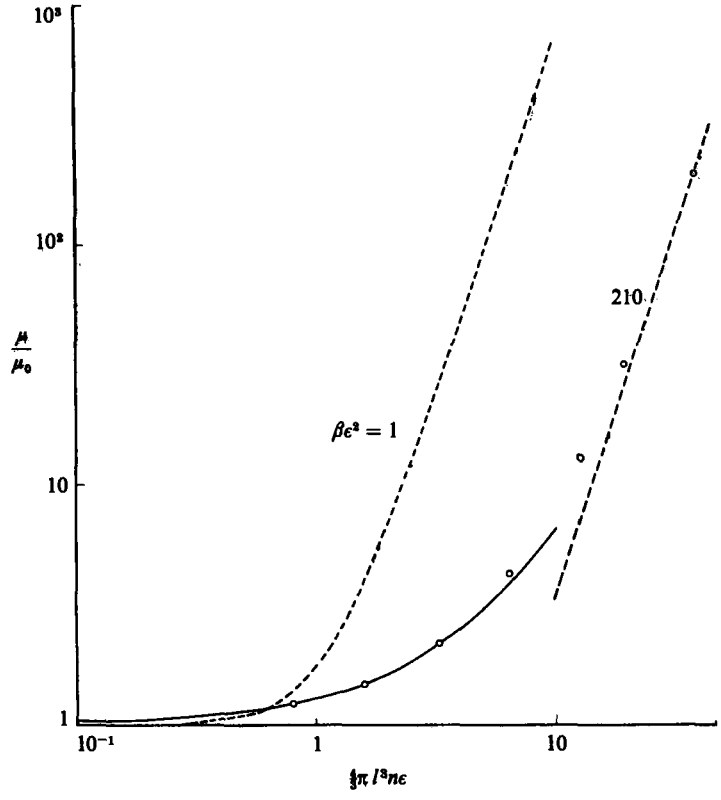


FIGURE 3. Low-shear limiting viscosity from pair-interaction theory (——) and semi-dilute theory of Doi & Edwards (1978*a*, *b*) (– – –) with data from Chauveteau (1982) for Xanthan gum (○).

For suspensions of spheres of radius $a$, $O(a^3n)^2$ theories remain reasonably accurate up to $\bar{\mu} \approx 1.4$–$2.0$. Indeed figure 3 shows that Chauveteau's (1982) data for Xanthan gum in the low-shear limit follows (56) for $\mu \leqslant 4$. Above $\bar{\mu} \approx 30$ the results conform to the semi-dilute theory if $\beta\epsilon^2 \approx 210$. This means $\beta \approx 8.6 \times 10^3$, contrary to the original assumption of Doi & Edwards (1978*a*) that $\beta = O(1)$ but consistent with dynamic light-scattering measurements (Pecora 1985).

Figure 4 shows the corresponding results for the first normal-stress difference. The ratios of the two normal stresses indicate a minor inconsistency between the two theories. From the semi-dilute theory $-N_2/N_1 = 2/7$, independent of concentration, while the dilute theory predicts this ratio to decrease from 1/7 with increasing concentration.

This comparison of the dilute and semi-dilute theories with viscosities measured for Xanthan gum solutions suggests that at near zero shear rates the dilute regime extends to $[\eta]_0 c \approx 1.5$–$1.75$ while the semi-dilute regime begins about $[\eta]_0 c \approx 5$–$6$. Some questions remain about the application of both theories since the molecular weight deduced from the former seems low and the value of $\beta$ required to fit the latter seems high.

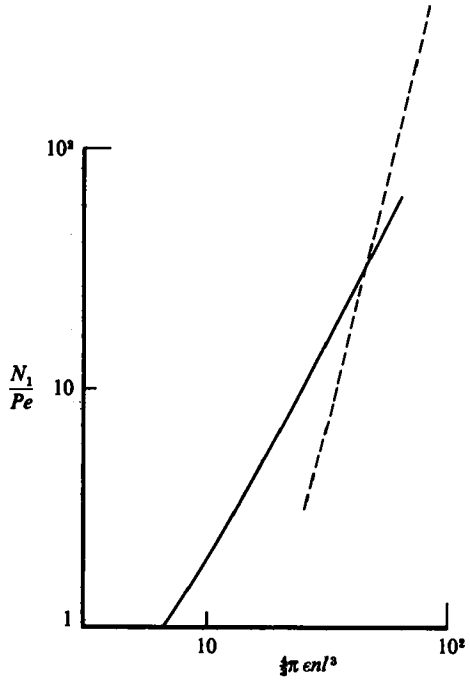


FIGURE 4. First normal-stress difference from pair-interaction theory (——) and semi-dilute theory of Doi & Edwards (1978*a*, *b*) with $\beta c^2 = 210$ (– – – –).

## 9. Summary

In this paper we have calculated the effects of far-field hydrodynamic interactions between rods on the orientational distribution and bulk stress for a general steady shear flow. The solutions, obtained to $O(Pe^3)$ as regular perturbation expansions, indicate that interactions increase the alignment of the rods with the flow and, thereby, enhance the shear thinning and strain thickening expected from dilute theories. In the Newtonian low-shear limit the Huggins' coefficient assumes the value of 0.40 found previously for free-draining coils.

The theoretical predictions for the Huggins coefficient agree qualitatively with data for Xanthan gum (Chauveteau 1982), a semi-rigid biopolymer. Quantitatively, the low-shear limit errs by only about 10 %, but the shear-rate dependence predicted for the Huggins coefficient is significantly less than observed.

The concentration dependence arising from pair interactions is, of course, much weaker than that resulting from semi-dilute theories. A brief comparison emphasizes further the fundamentally different nature of the interactions between the two and indicates the transition at near zero shear rates to occur for $1.5 \leqslant [\eta]_0 c \leqslant 6$.

This work was partially supported by the National Science Foundation through Grant CPE-7825929. The authors thank E. J. Hinch for key suggestions at several points along the way.

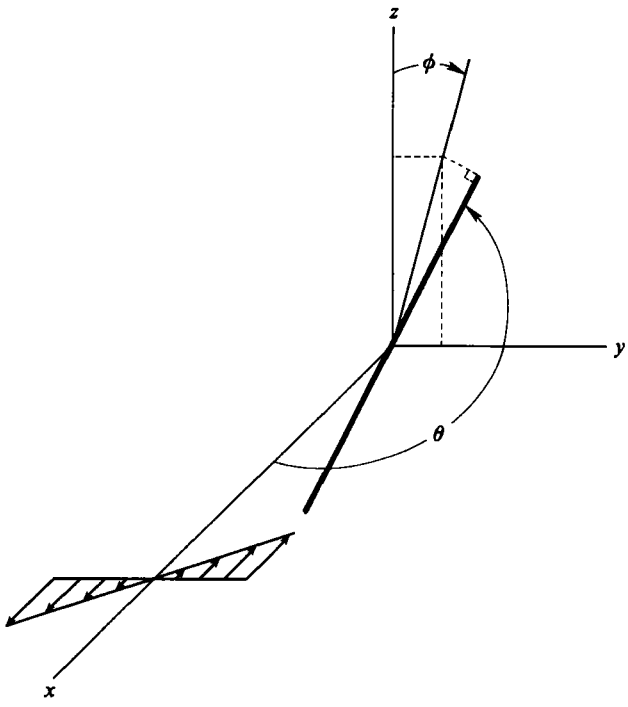


FIGURE 5. Polar angles relative to alignment direction for single rod in simple shear flow.

## Appendix. Basis vectors for calculation of $\langle \boldsymbol{I} \rangle$

In order to calculate the average moment of inertia $\langle \boldsymbol{I} \rangle$ in (34), the orientation vector $\boldsymbol{q}_2$ is expressed in a spherical coordinate system (see figure 5) containing $\boldsymbol{q}_1$ as

$$\boldsymbol{q}_2 = \sin\alpha\cos\beta\boldsymbol{\theta} + \sin\alpha\sin\beta\boldsymbol{\phi} + \cos\alpha\boldsymbol{q}_1. \tag{A 1}$$

The orientation vector $\boldsymbol{q}_1$ written in spherical coordinates with respect to a space-fixed coordinate system as

$$\boldsymbol{q}_1 = \sin\theta\cos\phi\boldsymbol{i}_1 + \sin\theta\sin\phi\boldsymbol{i}_2 + \cos\theta\boldsymbol{i}_3 \tag{A 2}$$

defines

$$\left.\begin{aligned} \boldsymbol{\theta} &= \cos\theta\cos\phi\boldsymbol{i}_1 + \cos\theta\sin\phi\boldsymbol{i}_2 - \sin\theta\boldsymbol{i}_3, \\ \boldsymbol{\phi} &= -\sin\phi\boldsymbol{i}_1 + \cos\phi\boldsymbol{i}_2, \\ \boldsymbol{q}_1 &= \sin\theta\cos\phi\boldsymbol{i}_1 + \sin\theta\sin\phi\boldsymbol{i}_2 + \cos\theta\boldsymbol{i}_3. \end{aligned}\right\} \tag{A 3}$$

The vector identities

$$\boldsymbol{q}_1 \times \boldsymbol{q}_2 = \sin\alpha\cos\beta\boldsymbol{\phi} - \sin\alpha\sin\beta\boldsymbol{\theta}$$

and

$$\theta_i\theta_j + \phi_i\phi_j = \delta_{ij} - q_i q_j \quad \text{(index notation)},$$

along with orthogonality relationships are then used in calculating $\langle \boldsymbol{I} \rangle$.

## REFERENCES


BATCHELOR, G. K. 1970*a* The stress system in a suspension of force-free particles. *J. Fluid Mech.* **41**, 545.

BATCHELOR, G. K. 1970*b* Slender body theory for particles of arbitrary cross-section in Stokes flow. *J. Fluid Mech.* **44**, 419.

BATCHELOR, G. K. 1971 The stress generated in a non-dilute suspension of elongated particles by a pure straining motion. *J. Fluid Mech.* **46**, 813.

BATCHELOR, G. K. 1976 Developments in microhydrodynamics. In *Theoretical and Applied Mechanics* (ed. W. T. Koiter), pp. 33–55. North-Holland.

BATCHELOR, G. K. 1977 The effect of Brownian motion on the bulk stress in a suspension of spherical particles. *J. Fluid Mech.* **83**, 97.

BATCHELOR, G. K. & GREEN, J. T. 1972 The determination of the bulk stress in a suspension of spherical particles to order $c^2$. *J. Fluid Mech.* **56**, 375.

BERRY, D. H. 1982 The rheological effects of hydrodynamic and electrostatic interactions in solutions of semi-rigid polyelectrolytes. Ph.D. dissertation, Princeton University.

BRENNER, H. 1974 Rheology of a dilute suspension of axisymmetric Brownian particles. *Intl J. Multiphase Flow* **1**, 195.

BRENNER, H. & CONDIFF, D. W. 1974 Transport mechanics in systems of orientable particles. IV. Convective transport. *J. Colloid Interface Sci.* **47**, 199.

CHAUVETEAU, G. 1982 Rodlike polymer solution flow through fine pores: Influence of pore size on rheological behavior. *J. Rheol.* **26**, 111.

CHU, S.-G., VENKATRAMAN, S., BERRY, G. C. & EINAGA, Y. 1981 Rheological properties of rodlike polymers in solution. 1. Linear and nonlinear steady state behavior. *Macromol.* **14**, 939.

DOI, M. & EDWARDS, S. F. 1978*a* Dynamics of rodlike macromolecules in concentrated solution. Part 1. *J. Chem. Soc. Faraday Trans. I* **74**, 560.

DOI, M. & EDWARDS, S. F. 1978*b* Dynamics of rodlike macromolecules in concentrated solution. Part 2. *J. Chem. Soc. Faraday Trans. I* **74**, 918.

FELDERHOF, B. U. 1976 Rheology of polymer suspensions. II. Translation, rotation, and viscosity. *Physica A* **82**, 596.

GIESEKUS, H. 1962 Elasto-viskose Flüssigkeiten, für die in stationären Schichtströmungen sämtliche Normalspannungskomponenten verschieden grosse sind. *Rheol. Acta.* **2**, 50.

HINCH, E. J. 1977 An averaged-equation approach to particle interactions in a fluid suspension. *J. Fluid Mech.* **83**, 695.

HINCH, E. J. & LEAL, L. G. 1972 The effect of Brownian motion on the rheological properties of a suspension of non-spherical particles. *J. Fluid Mech.* **52**, 683.

HOLZWARTH, G. 1978 Molecular weight of Xanthan polysaccharide. *Carbohydr. Res.* **66**, 173.

HOLZWARTH, G. & PRESTRIDGE, E. K. 1978 Multistranded helix in Xanthan polysaccharide. *Science* **197**, 757.

JAIN, S. & COHEN, C. 1981 Rheology of rodlike macromolecules in semidilute solutions. *Macromol.* **14**, 759.

MOAN, M. & WOLFF, C. 1974 Etude viscosimetrique de solutions de polyelectrolytes par dilution isoionique. Effet de la densité de charge sur la conformation du polyion. *Die Makromolekular Chemie* **175**, 2881.

PECORA, R. 1985 Dynamics of rodlike macromolecules in semi-dilute solutions. *J. Polymer. Sci.* C: **73**, 83.

RALLISON, J. M. & HINCH, E. J. 1986 The effect of particle interactions on dynamic light scattering from a dilute suspension. *J. Fluid Mech.* **167**, 131.

RUSSEL, W. B. 1979 The low-shear limit of the effective viscosity of a solution of charged macromolecules. *J. Fluid Mech.* **92**, 40.

RUSSEL, W. B. 1980 A review of the role of colloidal forces in the rheology of suspensions. *J. Rheol.* **24**, 287.

SCHERAGA, H. A. 1955 Non-Newtonian viscosity of solutions of ellipsoidal particles. *J. Chem. Phys.* **23**, 1526.

WHITCOMB, P. J. & MACOSKO, C. W. 1978 Rheology of Xanthan gum. *J. Rheol.* **22**, 493.